Lasers in Manufacturing Conference 2017

# Behavior of laser induced keyhole during dissimilar welding of metals

I. Tomashchuk[a,*] , M. Mostafa[b], T. Caudwell[a], P. Sallamand[a], M. Duband[a]

[a] *Laboratoire Interdisciplinaire Carnot de Bourgogne, Université de Bourgogne-Franche Comté, 71200 - Le Creusot, France*
[b] *Laser Tech. & Environment Lab, Faculty of Science, South Valley University, 83523 - Qena, Egypt*

**Abstract**

Keyhole behavior during laser welding highly influences the final composition and the shape of the weld, which determine resulting tensile strength. When different materials are welded together, the keyhole formation is likely to be affected by a mismatch in physical properties. Thus, quantifying and understanding the potential keyhole asymmetry and/or shift from joint line is important to choose appropriate welding conditions. To this end, novel experiments have been conducted: keyhole development has been monitored laterally through a quartz window using high-speed camera. Two couples of materials were studied: aluminum/magnesium and copper/steel. The first couple that has close absorption coefficients and fusion temperatures, so the keyhole develops preferentially in magnesium, presumably because of its lower boiling temperature and latent heat of vaporization. On the other hand, for copper/steel couple, the keyhole tends to shift from copper to steel, because of strong reflectivity of laser radiation and high thermal conductivity of copper. This tendency inverts if energy density of copper melting is overpassed: for high laser power keyhole tends to shift on copper side, because of lower boiling temperature and latent heat of vaporization.

Keywords: laser, keyhole, dissimilar welding

## 1. Introduction

During dissimilar welding of metals with high power laser sources, shape and position of vapor-filled keyhole strongly influence the characteristics of melted zone. For dissimilar couple of materials, the

* Corresponding author. Tel.: +33 03 85 73 11 23 .
*E-mail address:* iryna.tomashchuk@u-bourgogne.fr .

mismatch in physical properties can lead to an asymmetry of the keyhole and more or less strong shift from joint line (Torkamany et al, 2016). This has immediate consequences on shape and composition of the melted zone. Very few experimental studies quantify this phenomenon. Usually it is assumed that actual position of the keyhole coincides with laser beam position on joint line. However, this is generally not the case for the welding of dissimilar metals (Tomashchuk, 2010). For accurate choice of operational conditions, especially for welding of metallurgically incompatible combinations, it is important to know exact keyhole position and behavior.

Laser keyhole shape has been analyzed by several methods. Schneider, 2006 proposed a post-mortem method that consisted in performing laser drilling at the interface between polished metallic sheets and then measure the created cavities. Many authors used X-ray imagery (Arata et al, 1979, Fujinaga et al, 2000, Matsunawa et al, 2001) to visualize the behavior of the capillary during continuous welding, but they often faced insufficient image contrast and resolution. These issues were solved by X-ray phase-contrast method (Miyagi et al, 2016). Method of optical coherence tomography, recently introduced by Dorsch et al, 2016, showed interesting results for tracing real-time keyhole profile for a given range of keyhole sizes.

High speed imaging (HSI) is more and more used for the monitoring of melted surface during the welding. The interaction zone is illuminated by a diode laser, and a high speed camera acquires images at the consistent spectral band. This avoids image overexposition by laser-generated plasma plume. Using this method, Fabbro, 2011 described different keyhole regimes that depend on welding speed and laser power. Erikson et al, 2003 used image treatment to extract the shape of keyhole. Torkamany et al, 2016 also used HSI to quantify shift of keyhole center from joint line during welding of titanium with niobium. However, this approach only allows the observation of keyhole opening. Mostafa et al, 2010 performed cross-section observation of the keyhole in pure tin through optically transparent quartz sheet during both drilling and continuous welding. In this configuration, half of the beam is directed towards metal sheet and other half passes through quartz sheet with very little interaction, which allows approaching plane symmetry condition of keyhole observation. Mostafa, 2011 showed that the presence of the quartz sheet reduced the depth of the keyhole in pure tin of about 20% without changing global dynamics of keyhole-associated phenomena.

In the present study, HSI observation of the keyhole during dissimilar laser welding is performed in two configurations. First, HSI monitoring of the keyhole during continuous welding of copper with stainless steel is performed. Next, cross-section observation of keyhole formation through quartz sheet is performed for pulsed welding of aluminum with magnesium alloy. For both cases, the effect of operational parameters on keyhole shape and offset from joint line has been quantified. The method of cross-section observation for chosen materials is validated by comparison with method proposed by Schneider, 2006.

## 2. Experiments

Continuous welding experiments were performed with a Yb:YAG laser ($\lambda$=1053 nm) of 6 kW maximal power, focal distance of 200 mm and a spot diameter of 200 µm. 2 mm thick sheets of commercially pure copper and stainless steel 316L were butt-welded with laser focused on top surface (Figure 1.a). Top and bottom gas protection with 20 L/min argon flow was applied. All experiments resulted in fully penetrated welds. Three sequences of welds were performed:

- variation of laser power from 1 to 5 kW, welding speed of 1 m/min and laser spot centered on copper/steel interface;
- variation of welding speed from 0.5 to 3 m/min, constant laser power of 2 kW and laser spot centered on copper/steel interface;
- variation of laser spot offset from joint line from 500 µm shift on steel to 200 µm shift on copper, with constant laser power of 2 kW and welding speed of 2 m/min.

Distance marks have been previously made at 2 mm from welded edges to calibrate the videos. HSI acquisition was performed using camera Phantom V9.0, inclined to an angle of 33° from laser beam axis, with image resolution of 800x1200 px, exposure time of 3 µs and frequency of 500 img/s. The melted zone has been monitored for its total lifetime. The dimensions of weld end point have been measured by optical microscopy and compared with the last image of each video to compensate eventual image deformation by inclination angle and as a result to get correct scales on x and y axis. For statistical treatment of keyhole dimensions, 5 measures per condition were made, and confidence intervals have been estimated using Student law with bi-lateral risk of 5%.

Pulsed welding experiments were performed using a Nd:YAG laser (λ=1064 nm) of 3 kW maximal power, a focal distance of 200 mm and a spot diameter of 400 µm. Focused beam was positioned at the joint of quartz sheet and the interface between polished magnesium alloy AZ31 and aluminum alloy 5754. No gas protection was used. Half of the beam was situated on quartz side. High speed camera was facing Al/Mg interface through quartz window in order to obtain non-deformed side view of keyhole formation (Figure 1.b) with image resolution of 480x480 px, frequency of 6400 img/s and exposure time of 3 µs. For data treatment, 10 images of keyhole formation were processed. The operational parameters were chosen in order to approach drilling regime. 2.5 kW pulses of 6 ms were used for all welds. Laser beam offset from Mg/Al interface varied from -300 µm offset to Al to 300 µm offset to Mg, with step of 100 µm. In this way, seven positions of laser beam were tested. Additional acquisition with 10 ms pulse duration was carried out to confirm the results obtained in previous work (Mostafa et al, 2017). The comparison was made between Al/quartz and Al/Al configurations, as well as between Mg/quartz and Mg/Al, in order to quantify the effect of quartz on melted zone dimensions. Metal/quartz and metal/metal couples were splitted and dimensions of interaction zone were measured with optical microscopy. The physical properties of the materials are listed in Table 1.

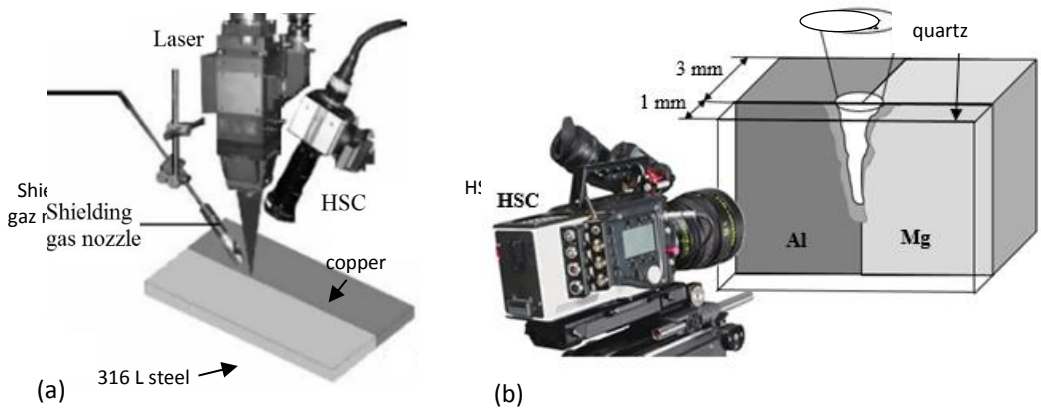


Fig. 1. Experimental setup for observation of a keyhole during (a) continuous and (b) pulsed welding configurations.

Table 1. Physical properties of materials

| Materials | Pure copper | 316L Steel | Mg AZ31 | Al 5754 | Quartz |
|---|---|---|---|---|---|
| Absorption coefficient | <0.03 | 0.3 | 0.3 | 0.3 | <0.05 |
| T solidus -T liquidus *(K)* | 1357 | 1648-1723 | 878-903 | 883-902 | 1830 |
| T vaporization *(K)* | 2835 | 3013 | 1380 | 2792 | 2473 |
| Latent heat of fusion *($kJ{\cdot}mol^{-1}$)* | 13.05 | 13.8 | 8.95 | 10.79 | 14.23 |
| Latent heat of vaporization *($kJ{\cdot}mol^{-1}$)* | 300 | 340 | 127 | 294 | 283 |
| Thermal diffusivity *($m^2/s$)* | $117{\cdot}10^{-6}$ | $3.8{\cdot}10^{-6}$ | $87.9{\cdot}10^{-6}$ | $98.8{\cdot}10^{-6}$ | $0.83^{\cdot 10-6}$ |

## 3. Results and discussion

### *3.1. Continuous welding of copper to stainless steel*

For three sets of continuous welding experiments, the dimensions of the keyhole opening and its offset from the joint line were measured. For all examined cases, the keyhole appears to be stretched along the joint line. This effect becomes more pronounced under high welding speeds (Fig 2). Because of high thermal diffusivity of copper, the melted zone has a strong tendency to shift on stainless steel. Elongated keyhole orients itself in the same way than melted zone, which reflects the morphology of generated thermal field (Tomashchuk, 2010).

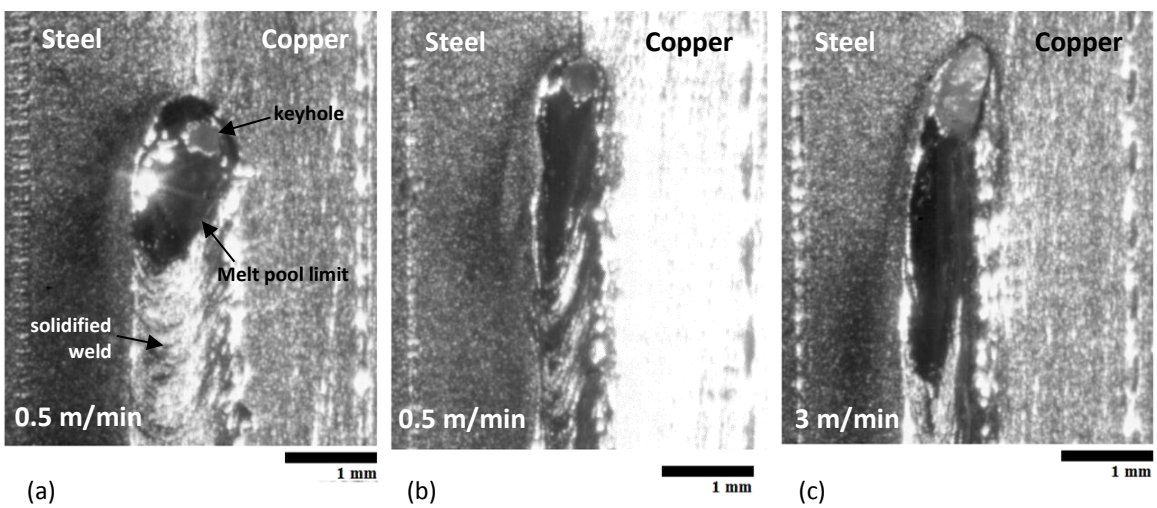


Fig. 2. Top view of keyhole opening and melt pool under various welding speeds (laser power of 2 kW, laser spot centered on copper/steel interface).

The increase of welding speed under condition of full penetration shows for dissimilar copper-steel welds the same regimes of keyhole evolution, that were revealed by Fabbro, 2011 for continuous laser welding on steel. For slow welding speed (0.5 m/min) Rosenthal regime of melted zone is observed (Fig 1.a): liquid surface is almost undisturbed. For welding speeds between 1 and 2.5 m/min, single wave regime is observed (Fig 1.b). These two regimes are characterized by a slight elongation of the keyhole (Figure 3.a). At 3 m/min elongated keyhole regime begins (Fig. 1.c): in this case keyhole maximal length doubles its width and the

opening of the keyhole happens periodically. It is interesting to notice that for laser power of 2 kW the keyhole center remains always shifted to copper side (Fig 3.b), and the dispersion in keyhole position reduces itself with increase of speed, reaching some stability at 2.5 m/min. The change of keyhole regime at 3 m/min increases again the dispersion of keyhole position to joint line, and it goes even farther on the copper side. The transition between different keyhole regimes happens for lower speed comparing with results of Fabbro, 2011 obtained for steel.

The increase of laser power from 1 to 4 kW within single wave regime (V = 2 m/min) leads to linear increase of keyhole dimensions, but at 5 kW some stabilization regime is attained : keyhole opening becomes smaller as greater part of laser radiation is lost through the bottom opening (Fig 4.a). The keyhole opening is systematically at least twice bigger than beam diameter (200 µm). However, from previous research of Fabbro, 2010 it is known that keyhole width reduces with depth and approaches beam diameter. Unfortunately, it is impossible to see keyhole root section in present experiment. Up to 4 kW the position of keyhole center is subjected to important fluctuations (Fig 4.b) and tends to shift towards copper with increase of laser power. These fluctuations are suddenly reduced when laser 5 kW power is reached.

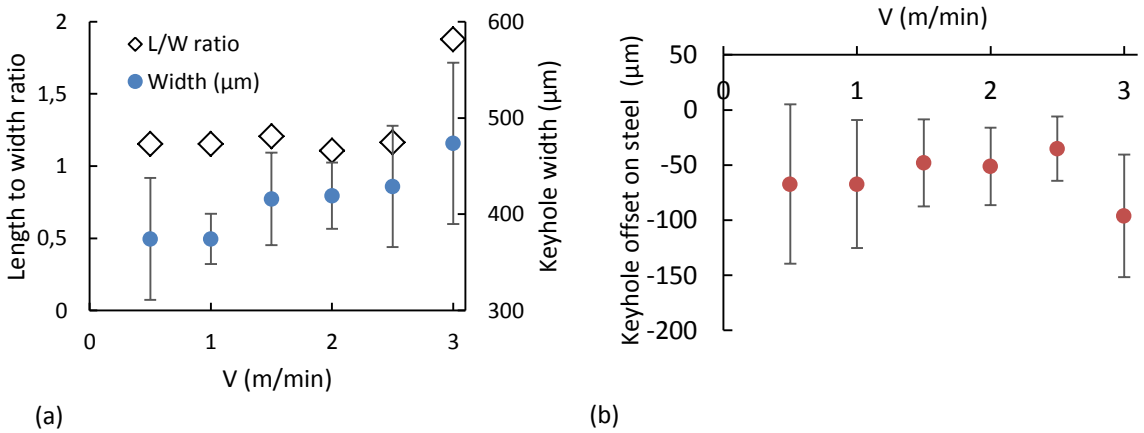


Fig. 3. Effect of welding speed on (a) keyhole dimensions and on (b) keyhole offset on steel (constant laser power of 2 kW and laser spot centered on copper/steel interface).

In previous study of Tomashchuk, 2010 the position of the keyhole for weaker laser powers was discussed (laser beam diameter and welding speed are the same that for Fig. 4). For laser power < 0.6 kW keyhole formation occurs only on steel side, then between 0.8 and 1.5 kW, keyhole progressively moves towards copper till reaching centered position (1.5 kW) and shifts at 50 µm towards copper under laser power of 2 kW, which is close to actual results. As solid copper has very low absorption coefficient of Yb:YAG laser radiation, the creation of symmetrical keyhole is associated with energy density estimated to $5 \cdot 10^{10}$ W/m². Above this value, the capillary tends to shift on copper side, having lower vaporization temperature and latent heat of vaporization.

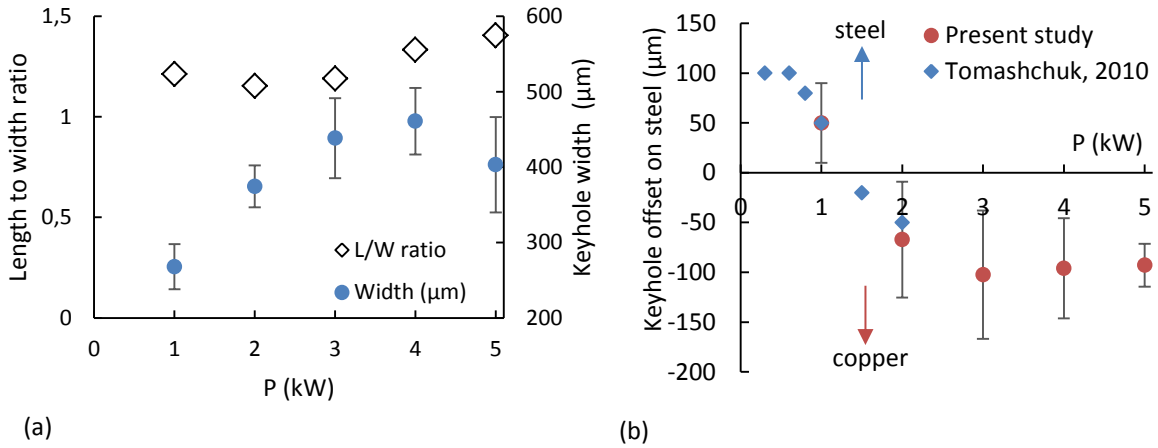


Fig. 4. Effect of laser power on (a) keyhole dimensions and (b) on keyhole offset on steel (constant welding speed of 1 m/min and laser spot centered on copper/steel interface).

The variation of laser beam offset from joint line showed that full-penetrated joint is possible only within the range from -200 µm (beam shifted on copper) to 500 µm (beam fully shifted on steel). In case of bigger offset on copper side, welding becomes impossible since the keyhole quits joint interface. From other side, twice bigger shift on steel still allows the formation of the joint. This is related to lower thermal diffusivity of steel. Larger melted zone is created and the joint is formed by strong brazing mechanism: melted steel enters in interdiffusion with solid copper wall. The shift of laser beam from copper to steel slightly increases keyhole width but does not induce significant modification of length to width ratio (Fig 5.a). The variation of actual position of keyhole center as a function of laser beam offset (Fig 5.b) shows that keyhole has a tendency to shift towards copper even for conditions when the beam and the keyhole are no longer situated in copper.

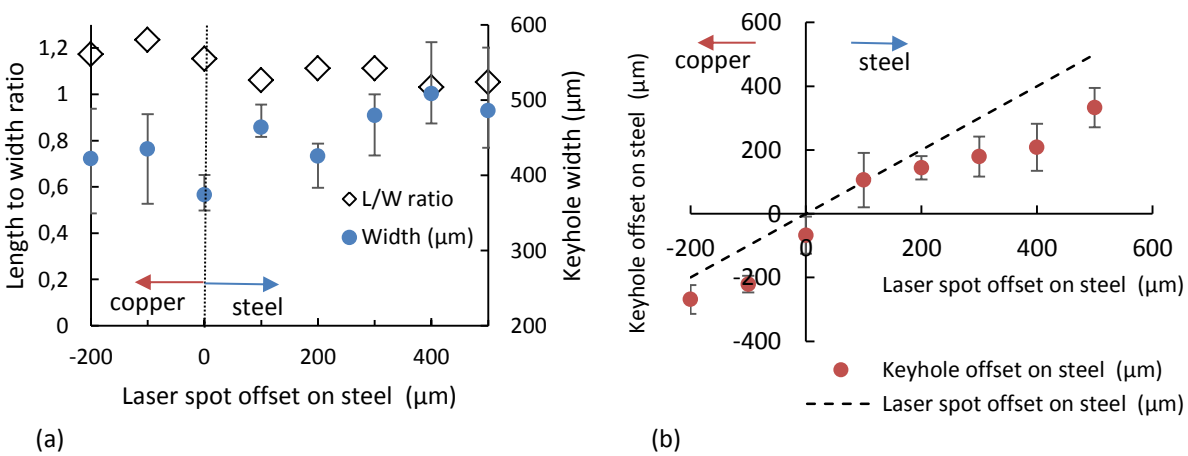


Fig. 5. Effect of laser spot offset from joint line on (a) keyhole dimensions and (b) keyhole offset on steel (constant welding speed of 1 m/min, laser power of 2 kW).

*3.2. Pulsed welding of aluminum to magnesium alloy*

In the first place, the effect of quartz sheet on weld dimensions in chosen materials has been quantified (Table 2). In case of metal/metal combinations, magnesium alloy AZ31 showed less large and deeper weld than aluminum alloy 5754. The contact with quartz enlarges the width of magnesium AZ 31 welds, but slightly increases the penetration. It produces opposite effect on aluminum alloy 5754: top width reduces, when penetration increases to >500 µm for chosen operational conditions. No notable ablation of quartz was noticed.

The visualization of keyhole development at Mg /Al interface was performed for different values of laser spot offset from joint line. Chosen laser parameters are close to drilling mode, which allows easier observation of the keyhole.

Keyhole development in case of centered beam position is shown on Fig 6. The limits of the keyhole are clearly visible and are surrounded by thin layer of melted matter. The top part of the image is darkened by shadow produced by top extremity of quartz plate.

Table 2. Comparison of weld dimensions produced in metal/metal and metal/quartz combinations (P = 2.5 kW, pulse duration of 6 ms).

| | Al/Al | Al/quartz | Relative gap (%) | Mg/Mg | Mg/quartz | Relative gap (%) |
|---|---|---|---|---|---|---|
| Width (µm) | 1299 ± 134 | 894 ± 90 | -31% | 829 ± 45 | 1017 ± 40 | 22 |
| Penetration (µm) | 2039 ± 90 | 2610 ± 375 | 28% | 5900 ± 260 | 6320 ± 217 | 7 |

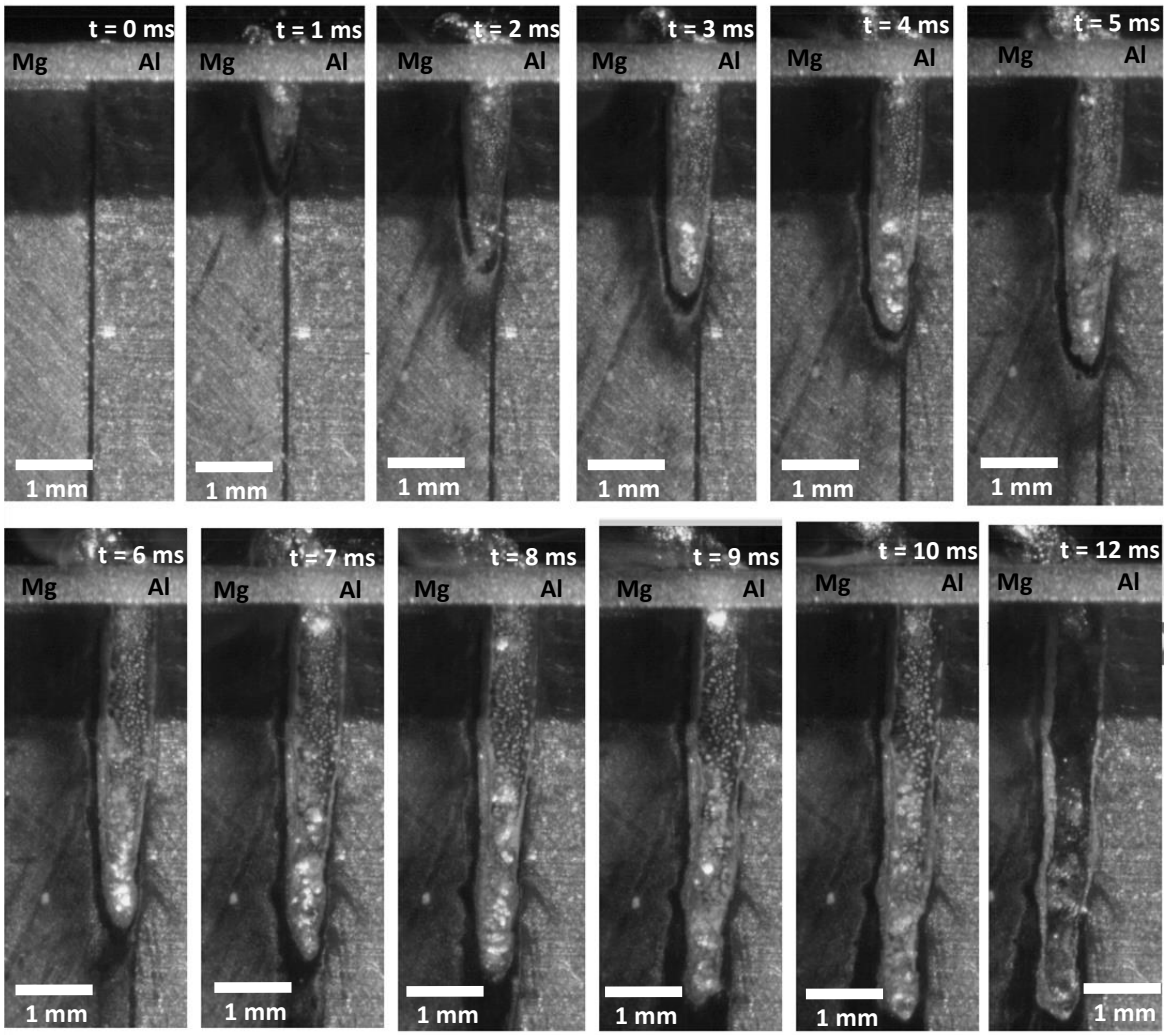


Fig. 6. Keyhole formation during 10 ms pulse at Mg /Al interface with laser power of 2.5 kW (beam spot of 400 µm).

The dimensions (Fig. 7.a) and the position (Fig 7.b) of the keyhole are strongly influenced by laser spot offset from joint line. For centered beam position, average width of the keyhole is twice bigger on Mg side than on Al side. This condition also corresponds to maximal depth: it can be supposed that beam alignment on joint line facilitates the creation of the keyhole because of the of a microscopic gap. Average total width and depth increase subsequently with laser offset on Mg side that has lower vaporization temperature and latent heat compared to Al. For the same reason, when laser beam is totally shifted to Al, the width of the keyhole is close to the diameter of laser spot (400 µm), and it overpasses 600 µm when laser spot is shifted on Mg side. Laser spot shift towards Mg does not induce important variations of depth and width of the keyhole comparing to centered position. The position of keyhole root is shifted on 100 µm to Mg side comparing to actual position of laser spot. Laser spot shift on Al side leads to important decrease of keyhole

width and depth. The position of keyhole root stagnates around joint line and shifts to actual laser spot position when the beam quits dissimilar interface.

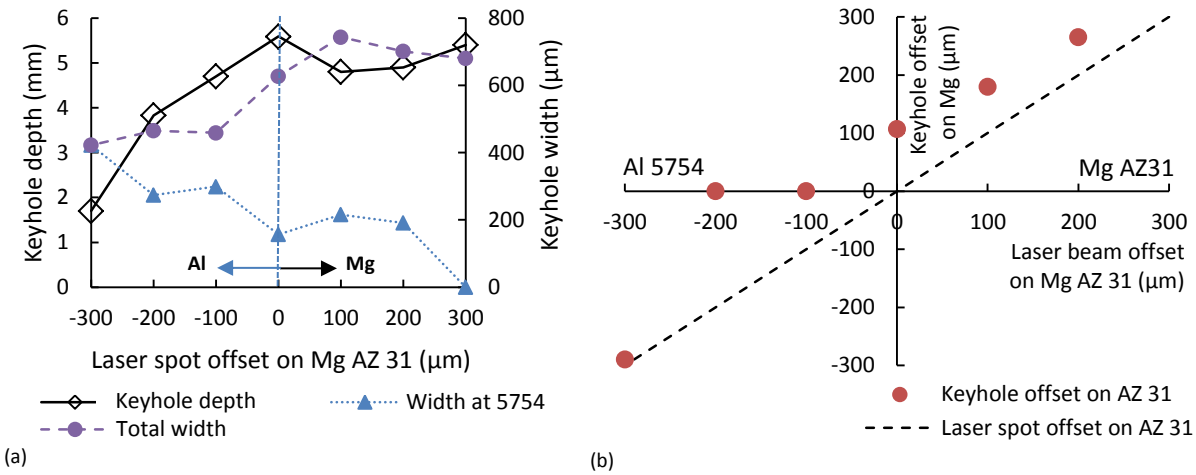


Fig. 7. Effect of laser spot offset from joint line on (a) keyhole dimensions and (b) keyhole offset from joint line during 6 ms pulse at Mg Al/Al interface with laser power of 2.5 kW (beam spot of 400 µm).

HSI analysis allows to follow the progression of keyhole drilling and to estimate the evolution of drilling rate (Fig. 8.a). The drilling process can be described by function of type $V_d = a \cdot t^{-b}$ and presents two stages. It starts at speed about 7 m/s and rapidly slows down to 1 m/min during first 2 ms. Then drilling continues to slow down and stabilizes around 0.5 m/min at the end of 10 ms interaction. According to our previous study (Mostafa et al, 2017), averadge drilling rate varies between condition of drilling of pure Mg (0.93 m/s) and of pure Al (0.28 m/s), depending of laser spot offset to joint line (Fig. 8.b).

### *3.3. Influence of physical properties of metals on keyhole development*

First considered couple, copper and stainless steel 316 L, have strong mismatch in solid absorption coefficient and thermal diffusivity. To compensate the difference in absorption coefficients, an energy density barrier must be reached (see 3.1), otherwise the keyhole remains shifted to the material with higher absorption coefficient. Thermal diffusivity does not seem to play an important role in keyhole formation, but it determines the proportion of materials in the melted zone (Tomashchuk, 2010). If the energy barrier is overpassed, keyhole has a tendency to shift to the material that has lower vaporization temperature and latent heat. The recoil pressure that builds in a keyhole is determined by partial pressures of vaporized elements. According to calculations of Alcock et al, 1984, copper creates higher vapor pressure than iron at given temperature (Table 3).

Table 3. Vapor pressure of various metals at 3000 K from data of Alcock et al, 1984 and Kaidalov, 2004.

| Liquid metals | Cu | Fe | Mg | Al | Ti | Nb |
|---|---|---|---|---|---|---|
| Vapor pressure (Pa) | $2.4 \cdot 10^5$ | $6.7 \cdot 10^4$ | $6.0 \cdot 10^7$ | $3.3 \cdot 10^5$ | $6 \cdot 10^3$ | 2.0 |

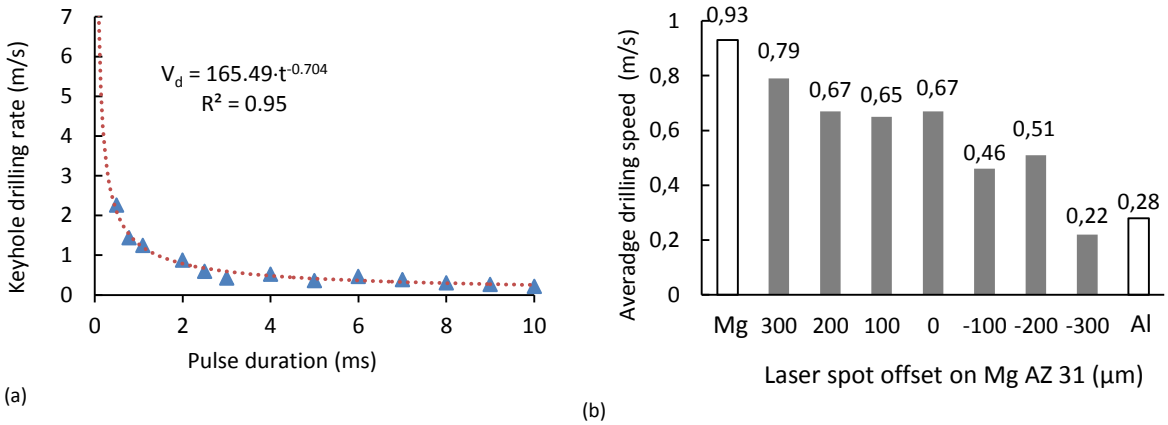


Fig. 8. Keyhole evolution at Mg/Al interface: (a) evolution of keyhole drilling rate for centered beam position (P = 2.5 kW, pulse duration 10 ms), (b) variation of drilling speed in function of laser spot offset from joint line (P = 2.5 kW, pulse duration 6 ms).

On the contrary, second couple of materials has close absorption coefficients and thermal diffusivities. However, the keyhole has a tendency to shift to Mg alloy, which has lower vaporization temperature and latent heat. The intensification of drilling process in presence of Mg can be explained by the fact that vapor pressure, which is responsible for keyhole opening, is higher for Mg (Table 3) and increases proportionally to the fraction of vaporized Al in Al-Mg system (Kaidalov, 2004).

The same tendency has been observed by Torkamany et al, 2016 for titanium-niobium couple, which has important mismatch in vaporization temperature and latent heat. For centered beam position the keyhole was totally shifted to titanium side. Estimated recoil pressure (Table 3) builds up preferentially on titanium side.

## 4. Conclusions

Top view HSI observation of keyhole and melted zone behavior during continuous welding of copper to stainless steel allows to follow keyhole fluctuations and evolutions of regime depending on welding speed. In spite of low absorptivity of laser radiation by copper, its involvement in keyhole formation is possible if specific energy barrier is overpassed. In studied conditions, keyhole has a tendency to shift towards copper side that has lower vaporization temperature and latent heat.

During lateral HSI observation of melted zone development through quartz window, carried out on alloys Mg AZ 31 and Al 5754, the dimensions of the capillary in pure materials are altered by contact with quartz, having different thermophysical and optical properties, so this method should be considered only after careful evaluation of this effect. However, it gives interesting results and possibility to observe the influence of laser spot shift from joint line on actual shift of the keyhole and to estimate drilling rate in different metals and metal combinations. It was shown that for magnesium/aluminum couple the keyhole also has a tendency to shift to the material with lower vaporization temperature and latent heat (here, magnesium AZ31).

Present results coherent with study of Torkamany, 2016 lead to conclusion that mismatch of these two parameters are of key importance for keyhole asymmetry to joint line. Absorption coefficient seems to be an important parameter for highly reflective materials, when the energy barrier should be overpassed to initiate the formation of the keyhole. The missmatch in thermal diffusivity plays secondary role. The keyhole shifts towards material that creates higher vapor pressure and thus contributes to internal recoil pressure. These

initial conclusions should be supported by additional experiments on different dissimilar couples presenting various mismatch of properties.

**Acknowledgements**

The authors would like to thank the Government of Egypt for funding the postdoctoral fellowship of M. Mostafa and to Dr Alexandre Mathieu (Laboratoire ICB, Université Bourgogne-Franche Comté) for his precious advices in realization of HSI.

**References**

Alcock, C. B., Itkin, V. P., and Horrigan, M. K., 1984, Vapour Pressure Equations for the Metallic Elements: 298–2500K, Canadian Metallurgical Quarterly, 23, p. 309.

Arata, Y., Abe, N., Oda, T., 1976, Dynamic behavior of laser welding and cutting, Proceeding of the Seventh International Conference on Electron and Ion Beam Science and Technology, p. 111.

Dorsch, F., Harrer, T., Haug, P., Plasswich, S., 2016, Process Control using capillary depth measurement, 9th International Conference on Photonic Technologies LANE 2016 , 19-22 September 2016, Fuerth, Germany.

Eriksson I., Powell J., Kaplan A.F.H., 2003, Melt behavior on the keyhole front during high speed laser welding, Opt Las Engineer, 51, p. 735.

Fabbro, R., 2011, Melt pool and keyhole behaviour analysis for deep penetration laser welding. Journal of Physics D: Applied Physics, IOP Publishing, 2010, 43 (44), p.445501.

Fabbro R., Chouf K., 2000, Dynamical description of the keyhole in deep penetration laser welding, Journal of Laser Applications, 12 (4), p. 142.

Fujinaga, S., Takenaka, H., Narikiyo, T., Katayama, S., Matsunawa, A., 2000, Direct observation of keyhole behavior during pulse modulated high-power Nd:YAG laser irradiation. J. Phys. D, 33, p. 492.

Kaidalov, A.A., 2004, Electron beam welding and annexed technologies (in Russian), Technologia, Kyiv.

Matsunawa, A. , Seto, N., Kim, J. D., Mizutani, M., Katayama, S., 2001, Observation of Keyhole and Molten Pool Behaviour in High Power Laser , Trans. of JWRI, 30–1, p. 13.

Miyagi, M., Kawahito, Y., Katayama, S., Kawakami, H., Shoubu, T., 2016, Observation of Keyhole and Melt Pool Dynamics in Laser Welding of Al Alloy by X-ray Phase-Contrast Method, Proc. International Congress on Applications of Lasers & Electro-Optics (ICALEO2016) #903, p. 1

Mostafa, M., 2011, Etude du perçage et du soudage laser : dynamique du capillaire, phD thesis Université de Bourgogne, France.

Mostafa, M., Jouvard, J.-M., Matteï, S., Andrzejewski, H., 2010, Etude des transferts d'énergie en soudage profond par laser en régime impulsionnel, SFT 2010, 24-28 mai 2010 – Le Touquet, France.

Mostafa M, Tomashchuk I, Caudwell T, Sallamand P, Duband M, 2017, Formation du capillaire de vapeur lors de l'interaction de laser de puissance avec la jonction dissimilaire Al-Mg, SFT 2017, 30 mai – 2 juin, Marseille, France.

Schneider, M., 2006, Perçage profond par laser : Analyse des processus physiques, phD thesis Université Pierre et Marie Curie - Paris VI, France.

Tomashchuk I., 2010. Assemblage hétérogène cuivre-inox et TA6V-inox par faisceaux de hautes énergies : compréhension et modélisation des phénomènes physico-chimiques, phD thesis Université de Bourgogne, France.

Torkamany, M.J., Malek Ghaini F., Poursalehi R., 2016, An insight to the mechanism of weld penetration in dissimilar pulsed laser welding of niobium and Ti–6Al–4V, Opt. & Las. Technol., 79, p. 100.